Simulation of the Unsteady Cavity Flow of the Stratospheric Observatory For Infrared Astronomy

Sven SCHMID[1], Thorsten LUTZ[2], Ewald KRÄMER[2]

[1]*German SOFIA Institute, Universität Stuttgart, Pfaffenwaldring 31*

[2]*Institute of Aerodynamics and Gas-Dynamics, Universität Stuttgart, Pfaffenwaldring 21*

70569 Stuttgart, Germany; Schmid@dsi.uni-stuttgart.de

Abstract: The flow around the Stratospheric Observatory For Infrared Astronomy SOFIA, a Boeing 747-SP with a 2.5 meter reflecting telescope was simulated with the Finite-Volume Solver TAU to compute pressure spectra at some selected locations on the telescope surface. Comparison of simulation data with data obtained by NASA in wind-tunnel tests reveal that the dominant resonance modes occurring in reality are captured by the URANS simulation. The frequencies of the modes are well predicted, a slight discrepancy can be observed regarding the amplitudes. The Helmholtz-equations were solved inside the telescope port with the 3D Finite-Element Solver NGSOLVE to compute frequencies and damping of acoustic modes. The spectral components at peak frequencies reveal a distinct similarity to acoustic modes, indicating that acoustic resonance is amplified by flow induced pressure oscillations. Passive flow control is performed at the SOFIA configuration by means of a slanted wall at the rear side of the telescope port where the shear layer spanning the opening reattaches the surface. The efficiency of mitigating fluctuations is demonstrated by comparing spectra to a configuration without control device, where peak amplitudes are distinctively higher.

Key words: cavity flow, URANS, shear layer, Helmholtz-equations, passive flow control.

1. Introduction

SOFIA is an airborne observatory to study the universe in the infrared spectrum. DLR and NASA modified a Boeing 747-SP to carry a 2.5 meter reflecting telescope for astronomical remote sensing purposes. During flight in the stratosphere, a door in the rear part of the fuselage opens to expose the telescope to the free atmosphere (see Figure 1). The telescope can be tilted to elevation

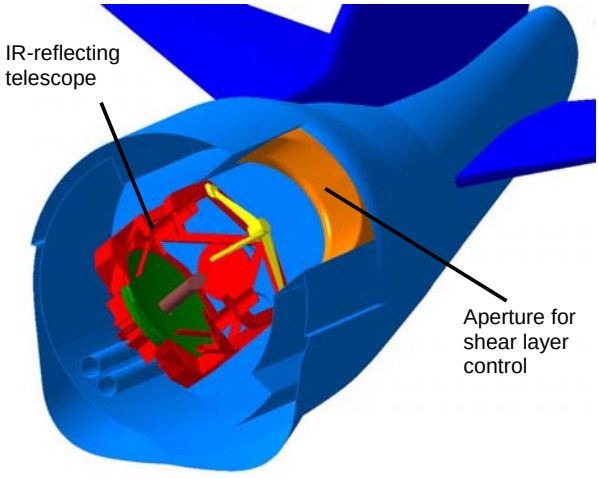

Figure 1: SOFIA - telescope inside the fuselage

angles of 20° - 60°, depending on the object to be observed. The success of the project depends mainly on the performance of the telescope and its image stability. Unsteady pressure loads, arising due to the interaction of shear layer disturbances with the interior of the port, lead to unwanted vibrations of the telescope structure and induce jitter. To minimize these adverse fluctuations, NASA optimized the geometry of a shear-layer control aperture located above the downstream bulkhead by means of extensive wind-tunnel studies in the transonic 14 ft wind tunnel in Ames/California [11]. A D-shaped geometry with a slant angle of about 30° was found to perform best for several flight conditions and different elevation angles.

This paper presents the results of steady and unsteady RANS simulations in comparison to experimental data. Coupling of unsteady shear-layer oscillations with acoustic resonance was investigated, acoustic eigenvectors were computed by solving the Helmholtz-equations. The effectiveness of the applied shear-layer control device is demonstrated by comparing solutions of the SOFIA configuration with a reference configuration without shear-layer control device.

2. Physics of Unsteady Cavity Flow and Acoustics

Cavity flow in general is characterized by self sustained pressure fluctuations [4, 12]. The shear layer spanning the opening of the cavity amplifies flow disturbances that are scattered into acoustic waves at the downstream corner (see Figure 2). These acoustic waves propagate upstream inside and outside the cavity and excite further disturbances in the shear layer, creating a feedback loop. Frequencies with a phase lag of a multiple of 2π are being amplified in particular, yielding the selection of discrete tones. Rossiter [12] states that the frequencies can be described by the semi empirical equation

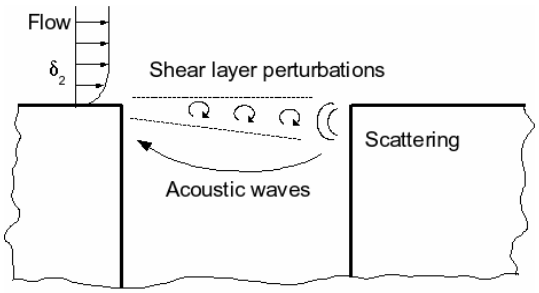

Figure 2: Cavity feedback mechanism

$$F = (U/L)\,(m-\gamma) / (1/K+Ma) \qquad m = 1,2,3... \tag{1}$$

where f is the frequency of the mode m, L is the reference length, Ma the Mach number. γ and K are empirical constants, representing the phase delay of disturbances that are scattered at the downstream corner and the average convection speed (relative to free stream velocity U) of disturbances in the shear layer. Rossiter found out empirically, that values of $\gamma = 0.25$ and $K = 0.57$ yield best agreement with measurement for many cavity configurations. The existence and the magnitude of these Rossiter modes depends basically on the stability characteristics of the shear layer that evolves from the boundary layer upstream

of the cavity [13], a crucial parameter is the momentum thickness divided by the cavity length δ_2/L. Small values lead to stronger shear-layer disturbance amplification and hence to higher fluctuation levels inside the cavity. Rossiter modes transport energy from the external flow into the cavity. If acoustic resonance frequencies of the cavity are close to these Rossiter frequencies, fluctuation levels are further increased as Rossiter modes trigger acoustic standing waves and lock in at the corresponding resonance frequencies [3, 6].

2.1. PASSIVE SHEAR-LAYER CONTROL

A steady stagnation point flow in a shear layer is skewed relative to the surface on which it impinges [7], i.e. it is not perpendicular to the surface (see Figure 3). Streamlines on opposite sides of the stagnation streamline need to be curved with different radii to guarantee pressure balance between both sides. In order to have a steady stagnation point on the rear bulkhead of a rectangular cavity, the shear layer must curve over the cavity length to achieve the proper impingement angle. However, a curved shear layer will be unsteady since there is no way to balance the resulting pressure difference which arises from curving the freestream flow. By slanting the rear bulkhead surface, the anticipated impingement angle can be achieved for a straight shear layer. The shape of the aperture (see Figure 1) was optimized by NASA in several wind-tunnel studies to fit the proper inclination angle in order to stabilize the shear layer [18]. Moreover, the aperture lip, extending into the port slightly below the shear layer, deflects perturbations to the exterior and prevents them from re-amplifying the shear layer. The feedback mechanism is alleviated by the weakening of the acoustic scattering process. In addition, the boundary layer downstream of the shear layer stagnation point on the aperture is accelerated due to the convex shape, increasing stability further.

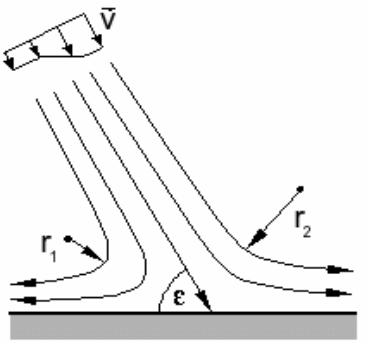

Figure 3: Shear layer impingement

Passive control of cavity flow by thickening of the upstream boundary layer has also been performed successfully by several authors [1, 7, 10, 12, 19]. The shear layer spanning the opening evolves from the boundary layer upstream of the cavity. Altering of the boundary layer thickness leads to changes of the shear layer's stability characteristics. Thicker shear layers in general are characterized by a more stable behaviour, whereas thinner shear layers amplify disturbances stronger. Rowley [13] and Ahuja et al. [1] showed, that unsteady pressure fluctuations can be nearly eliminated by increasing the boundary-layer thickness beyond a certain threshold. Unfortunately the thickening of the boundary layer increases the drag of the aircraft and is not considered in this investigation.

3. Simulation Methods

In the present investigations unsteady RANS computations were performed with the Finite-Volume RANS-solver TAU, that was developed by the Institute of Aerodynamics and Flow Technology of DLR [5]. The code solves the unsteady, compressible, three-dimensional Reynolds-averaged Navier-Stokes equations on unstructured or hybrid grids. Different cell types can be applied to account for different flow situations. Structured prismatic cells allow for high resolution in boundary layers with strong gradients in wall normal direction, tetrahedral elements facilitate the automation of the meshing procedure for complex geometries.

The computations presented here were performed applying the central-difference algorithm with second- and fourth-order numerical dissipation according to Jameson. Time accurate simulations were carried out by a dual time stepping scheme (DTS) that allows for convergence acceleration techniques like multigrid and residual smoothing. Flow turbulence was modelled by the Wallin EARSM turbulence model that has shown best performance compared to other turbulence models in previous cavity flow studies carried out by the present authors [15].

To investigate the acoustic resonance patterns of the cavity, the 3D Finite Element Solver NGSOLVE [16] by Joachim Schöberl from Johannes Kepler University of Linz was used. The Helmholtz-equations were solved inside and outside the cavity to compute frequencies and radiation losses of acoustic resonance modes. Perfectly Matched Layer (PML) boundary conditions were specified to avoid unphysical reflections at the grid boundaries [6]. Mean flow effects were neglected as the Mach number inside the cavity is supposed to be low. The real part of the computed eigenvectors corresponds to the resonance frequency, the imaginary part is a measure for the radiation loss of the corresponding mode. Acoustic modes with a low imaginary part are more likely to be pronounced as they accumulate more of the supplied energy.

For the URANS simulation a hybrid mesh around the 7% wind-tunnel model of the complete SOFIA aircraft-configuration including the telescope assembly was created with the commercial software GRIDGEN by Pointwise®. It consists of 23.0E+6 cells in total, about 8.9E+6 prisms were created to resolve the boundary layer on all viscous walls except the telescope surface, 14.1E+6 tetrahedrons fill up the rest of the computational domain. In order to resolve the boundary layer that evolves on viscous walls appropriately, a y^+ value of 1 was aimed at the first cell on the surfaces that are covered with prismatic cells. The prism stacks contain 38 prism layers in wall-normal direction, the boundary layer in important regions is resolved by 30-35 cells. A fully unstructured mesh containing 45.0E+3 tetrahedrons was generated for the cavity including the telescope to compute acoustic modes with NGSOLVE.

4. Flow Around the SOFIA Wind-Tunnel Model

The present CFD-results were compared to experimental data from the NASA wind-tunnel investigations [11] and flight tests [2]. As the boundary layer that develops upstream of the cavity has a strong influence on the unsteady flow inside the cavity, the computed pressure distribution and velocity profiles at relevant positions were compared to experimental data. The objective of this preliminary investigation was to ensure that the most important parameters that drive the cavity flow physics coincide in measurement and computation. The boundary layer was measured in wind tunnel along two rakes under 20° and 80° elevation upstream of the cavity. The agreement between computation and measurement is almost perfect for the rake placed at 80°. At 20° the computation predicts a slight lower velocity defect (see Figure 4). It should be mentioned that free-stream boundary-conditions were applied and no attempt was made to model the slotted walls of the wind tunnel, what might be an explanation for the discrepancy.

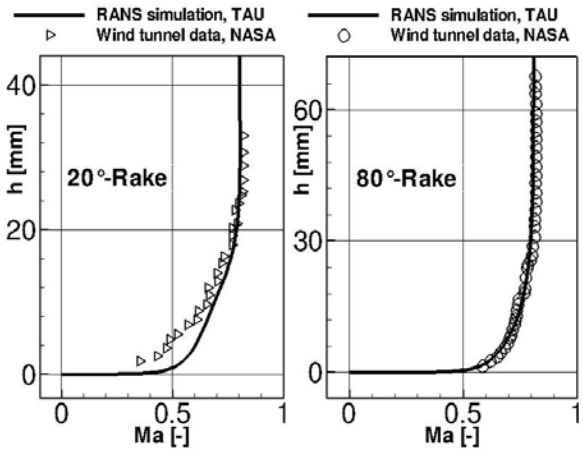

Figure 4: Boundary-layer profiles at 20° and 80° elevation upstream of the cavity

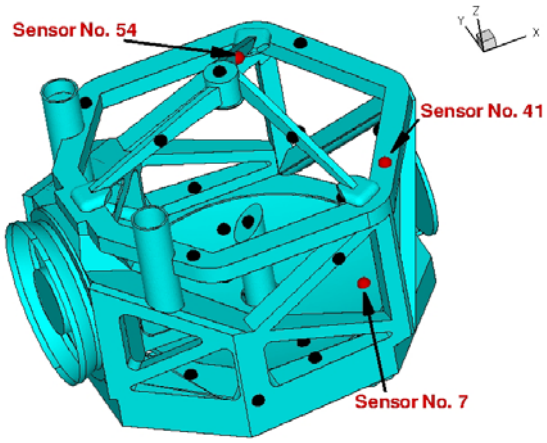

Figure 5: Sensor positions on telescope structure

The unsteady pressure history was measured by NASA in wind-tunnel investigations [8] by means of Kulites at 56 different locations on the surface of the telescope structure (see Figure 5). The URANS computations that were carried out in the present study started from a steady state solution. About 4700 time steps with 120 inner iterations per step were computed to initialize the unsteady flow field. After reaching a nearly periodic state, pressure data of 1000 time steps was used to generate the spectra. Figure 6 shows the result for 3 selected sensors on the telescope surface that demonstrate the different prevailing flow-induced and aero-acoustical effects. The low-frequency peak at about 3 Hz is caused by a Helmholtz-mode as the corresponding wavelength is beyond the

cavity dimensions [9]. The measured differences in magnitude between all sensors is quite low, pointing out that it can be described as a homogeneous „breathing“ of the cavity. Its contribution to the excitation of telescope vibrations is negligible as the resulting forces compensate.

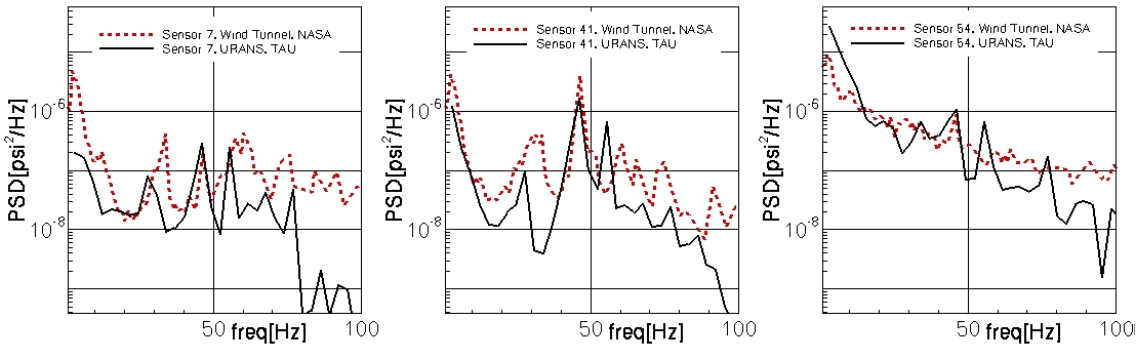

Figure 6: Power spectral density plots for sensor No. 7, 41 and 54

The second, third and fourth peaks are close to the analytically predicted frequencies of the first, second and third Rossiter modes. Table 1 compares measured with computed frequencies.

Table 1: Computed and measured peak frequencies

	Peak No. 2:	**Peak No. 3:**	**Peak No. 4:**
Rossiter equation (1), m = 1,2,3	~ 24 [Hz]	~ 47 [Hz]	~ 71 [Hz]
Measurement NASA (Sensor No. 7, 41)	~ 32 [Hz]	~ 45 [Hz]	~ 61 [Hz]
CFD solution DSI (Sensor No. 7, 41)	~ 28 [Hz]	~ 45 [Hz]	~ 57 [Hz]

Measured and computed peak frequencies coincide well with frequencies predicted by the semi empirical Rossiter equation (1), approving that these peaks correspond to the first three Rossiter modes. The second Rossiter mode could be identified in the CFD data by computing the phase difference of pressure disturbances. As already mentioned in Section 2, disturbances at frequencies with phase lags of a multiple of 2π along the feedback path are amplified exceptionally. The phase lag at 45 Hz along the shear layer and back inside the cavity slightly below the shear layer is about 4π.

Comparing the characteristics of the three sensor spectra, it becomes obvious that the spectrum of Sensor No. 54 is characterized by a broadband distribution whereas sensor No. 7 is dominated by more discrete tones. This finding can be observed in the simulation and in the experimental data as well. Streamlines and surface-pressure contour plots indicate that sensor No. 54 is located in a region with high convective velocities whereas sensor No. 7 and No. 41 lie in regions

where fluid-resonant effects dominate. Good accordance of the peak frequencies reveal that the physics of the driving cavity flow mechanisms is well resolved, at least up to a frequency of 70 Hz. The amplitude decline at higher frequencies is caused by the high diffusion of the second order FV-scheme. The general discrepancy of peak amplitudes is still an open issue and will be investigated in further studies. It is assumed that the differences can partly be attributed to the inadequacies of the URANS-assumptions. A further explanation could be the fact that the periodic state was not fully reached in the simulations.

As the Rossiter-frequencies are close to the acoustic resonance modes of the cavity, the presence of standing waves inside the cavity is evident and can be proved by considering spectral components of computed pressure fluctuations. Acoustic eigenvectors were computed with the 3D Finite-Element code NGSOLVE, the resulting patterns reveal a distinctive similarity to the URANS based fluctuation patterns. Figures 8-11 show the computed acoustic eigenvectors and the URANS based pressure-fluctuation patterns for 45 Hz and 57 Hz. The agreement between both patterns proves the presence of amplified standing acoustic waves.

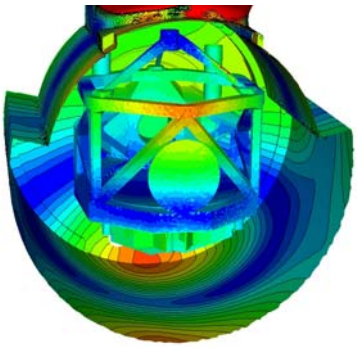

Figure 8: Fluctuation pattern 45 Hz (URANS, TAU)

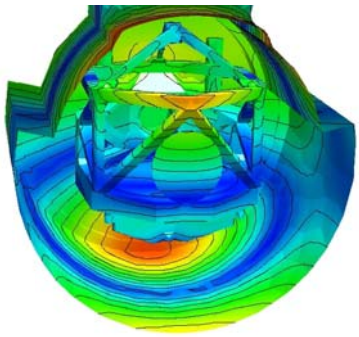

Figure 9: Acoustic eigenvector 45 Hz (NGSOLVE)

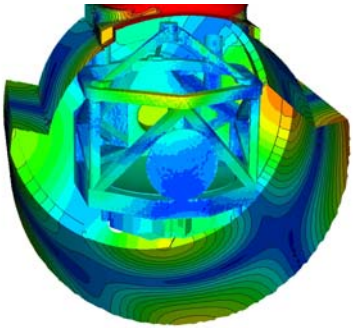

Figure 10: Fluctuation pattern 57 Hz (URANS, TAU)

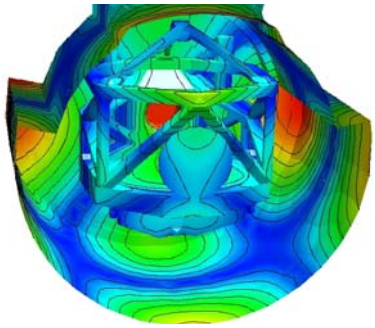

Figure 11: Acoustic eigenvector 57 Hz (NGSOLVE)

4.1. FLOW WITHOUT SHEAR-LAYER CONTROL

In order to study the effectiveness of the shear-layer control concept of the SOFIA-configuration, the flow around the identical configuration but without aperture was simulated. The slanted aperture surface at the shear-layer attachment region was substituted by a flat, nearly vertical plate (see Figure 12). The effective length of the cavity was increased from about 3.4 m to about 3.8 m. Snapshots of the vorticity distribution along the cavity shear-layer show the difference between both flow states. The shear layer

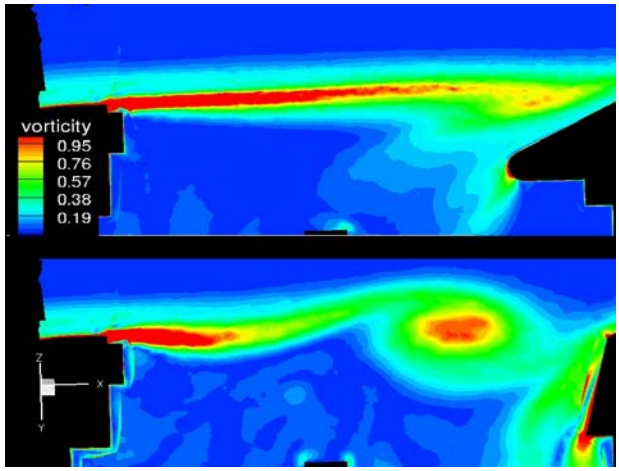

Figure 12: Vorticity distribution with/without passive shear-layer control

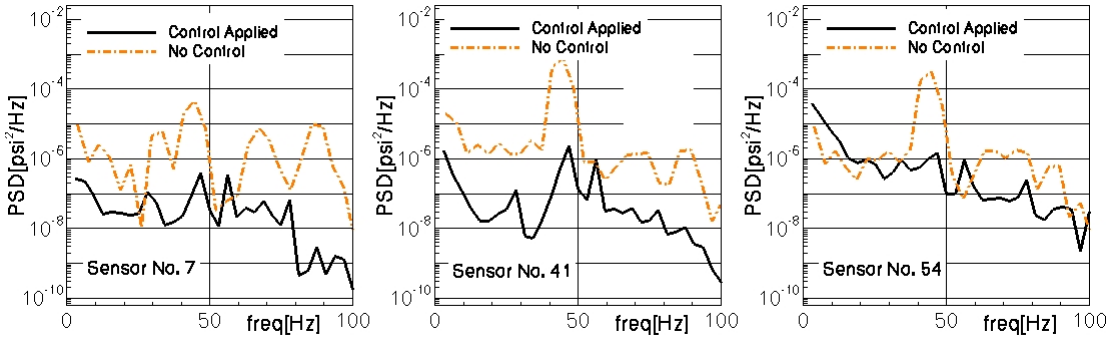

Figure 13: Pressure spectra for sensors No. 7, 41 and 54 with/without passive control

shows a quite stable behaviour when the aperture ramp is present. No roll-up of vortices can be observed, straight streamlines span the opening of the telescope port. By removing the aperture, the stagnation point of the shear layer starts to oscillate and the formation and convection of large-scale vortices is observed. The Mach-number inside the cavity is significantly increased, more energy from the exterior flow is entrained and fed into the cavity. High amplitude pressure fluctuations are the result of the

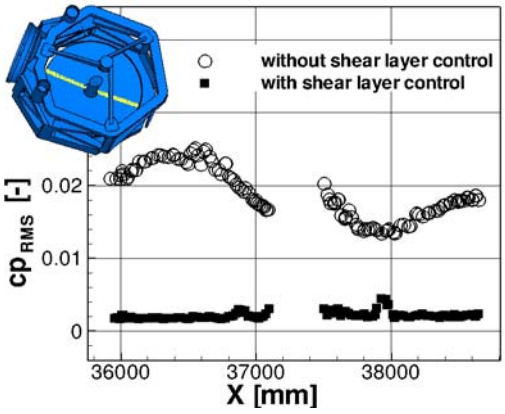

Figure 14: Overall pressure fluctuation on primary mirror surface (along yellow line)

reinforced feedback caused by the removal of the aperture. Pressure spectra computed for sensors No. 7, 41 and 54 (see Figure 13) show a prominent increase of unsteady fluctuations compared to the original configuration with applied shear-layer control. The peak at about 45 Hz is emphasized in particular. The increase of the cavity length also effects the frequency of the modes. In accordance to equation (1), the central peak frequency decreases. Nearly at all sensor positions the frequency of the second Rossiter mode drops from a value of about 45 Hz to about 43 Hz.

The favourable effect of the aperture on the pressure fluctuation on the telescope surface is further demonstrated in Figure 14. The RMS-values of unsteady pressure distribution on the primary mirror centerline (indicated by a yellow line) are plotted for both configurations and show a distinctive decrease of fluctuation magnitude due to the presence of the aperture.

5. Conclusions

Results of URANS computations of the flow around the Stratospheric Observatory For Infrared Astronomy SOFIA with and without passive shear-layer control are presented. Steady and unsteady data from simulation compares well with experimental data. Rossiter modes and amplified acoustic resonances could be identified as the cause of the discrete peaks at 35 Hz, 45 Hz and 57 Hz in the pressure spectra. Eigenvectors of acoustic computations basing on the solution of the Helmholtz-equations and the distribution of pressure fluctuations resulting from URANS simulations yield similar characteristic patterns.

The shear layer spanning the cavity mouth is attached to and stabilized by the shear-layer aperture, yielding stable flow conditions with low unsteady pressure fluctuations. When the aperture is removed, large scale vortex roll-up can be observed along the shear layer, leading to high-amplitude pressure loads inside the cavity. This fact points out the effectiveness of the shear-layer control system that was developed and optimized by NASA. The numerical simulation will be a helpful means to understand the physics of the flow and the acoustics inside the SOFIA cavity to further increase the telescope’s performance.

Acknowledgements

The authors like to thank Mr. Nans Kunz from NASA Ames and Mr. Bill Rose from Rose Engineering & Research INC. for their friendly collaboration and the supply of necessary data.

This project, grant Id 50 OK 0401, is being conducted on behalf of the German Aerospace Center (DLR) and supported with funds of the Federal Ministry of Economics and Technology (BMWi), the state of Baden-

Württemberg and of the Universität Stuttgart. The author is responsible for the content.

References

[1] K.K. Ahuja, J. Mendoza. “Effects of Cavity Dimensions, Boundary Layer, and Temperature on Cavity Noise With Emphasis on Benchmark Data To Validate Computational Aeroacoustic Codes”. NASA Contractor Report 4653, 1995.

[2] C. Atwood, W. Dalsem. “Flowfield Simulation About the Stratospheric Observatory For Infrared Astronomy”. Journal of Aircraft, Vol. 30, No. 5, 1993, pp. 719-727.

[3] P.J.W. Block. “Noise Response of Cavities of Varying Dimensions at Subsonic Speeds”. NASA Technical Note NASA TN D-8351, Washington 1976.

[4] N. Forestier, J. Laurent, L. Jacquin, P. Geffroy. “The mixing layer over a deep cavity at high-subsonic speed”. Journal of Fluid Mechanics, Vol. 475, 2003, pp. 101-145.

[5] T. Gerhold. ”Overview of the Hybrid RANS Code TAU”. In: N. Kroll et al. (Ed.) “MEGAFLOW - Numerical Flow Simulation for Aircraft Design”. NNFM, Vol. 89, Springer 2005, pp. 81-92.

[6] S. Hein, W. Koch. “Acoustic Resonances in a 2D High Lift Configuration and 3D Open Cavity”. American Institute of Aeronautics and Astronautics Paper 2005-2867.

[7] H. Heller, D. Bliss. “The Physical Mechanism of Flow-Induced Pressure Fluctuations in Cavities and Concepts for their Suppression”. In: AIAA 2nd Aero-Conference, Hampton, VA./March24-26, 1975, no. AIAA 75-491, 1975.

[8] M. McIntyre. “SOFIA V Pressure Sensor Power Spectral Density Plots”. SOFIA Technical Note TN MJM-007, 1999.

[9] M. McIntyre. “Analysis of SOFIA Cavity Acoustic Modes”. SOFIA Technical Note TN MJM-011, 2000.

[10] P. Nayyar, G. Barakos, K. Badcock und B. Richards. “Noise Suppression Methods for Transonic Cavity Flows”. Tech. Rep., CFD Laboratory, University of Glasgow, Glasgow, G12 8QQ, UK, pnayyar@aero.gla.ac.uk.

[11] Rose Engineering & Research, INC. “SOFIA V Design Validation Test Final Report”. Internal Report, 1998.

[12] J. E. Rossiter. “Wind-Tunnel Experiments on the Flow over Rectangular Cavities at Subsonic and Transonic Speeds”. R. & M. No. 3438, Ministry of Aviation, London 1966, pp. 1-32.

[13] C. W. Rowley. “Modeling, Simulation and Control of Cavity Flow Oscillations”. Thesis by Clarence W. Rowley, California Institute of Technology Pasadena, California, 2002.

[15] S. Schmid, Th. Lutz, E. Krämer. “Numerical Simulation of the Flow Field Around the Stratospheric Observatory For Infrared Astronomy”. To be published in NNFM. 15. DGLR Fach-Symposium der STAB, 29.11. - 01.12., TU Darmstadt.

[16] J. Schöberl. “NETGEN An advancing front 2D/3D-mesh generator based on abstract rules”, Computing and visualization in science, Vol. 1, 1997, pp. 41-52.

[17] G.R. Srinivasan, S.P. Klotz. “Features of Cavity Flow and Acoustics of the Stratospheric Observatory For Infrared Astronomy”, FEDSM97-3647, 1997.

[18] G.R. Srinivasan. “Influence of Cavity Aperture and Telescope Shape on Acoustics and Unsteady Flow of the Stratospheric Observatory for Infrared Astronomy”. Tech. Rep., NASA Ames Research Center, 1997.

[19] L. S. Ukeiley, M. K. Ponton, J. M. Seiner und B. Jansen. “Suppression of Pressure Loads in Cavity Flows”. AIAA Journal, Vol. 42, No. 1, S. 70–79, Januar 2004.